OPEN ACCESS Freely available online

PLOS ONE

Neuronal Spike Initiation Modulated by Extracellular Electric Fields

Guo-Sheng Yi[1], Jiang Wang[1], Xi-Le Wei[1]*, Kai-Ming Tsang[2], Wai-Lok Chan[2], Bin Deng[1]

1 School of Electrical Engineering and Automation, Tianjin University, Tianjin, China, **2** Department of Electrical Engineering, The Hong Kong Polytechnic University, Hong Kong, China

Abstract

Based on a reduced two-compartment model, the dynamical and biophysical mechanism underlying the spike initiation of the neuron to extracellular electric fields is investigated in this paper. With stability and phase plane analysis, we first investigate in detail the dynamical properties of neuronal spike initiation induced by geometric parameter and internal coupling conductance. The geometric parameter is the ratio between soma area and total membrane area, which describes the proportion of area occupied by somatic chamber. It is found that varying it could qualitatively alter the bifurcation structures of equilibrium as well as neuronal phase portraits, which remain unchanged when varying internal coupling conductance. By analyzing the activating properties of somatic membrane currents at subthreshold potentials, we explore the relevant biophysical basis of spike initiation dynamics induced by these two parameters. It is observed that increasing geometric parameter could greatly decrease the intensity of the internal current flowing from soma to dendrite, which switches spike initiation dynamics from Hopf bifurcation to SNIC bifurcation; increasing internal coupling conductance could lead to the increase of this outward internal current, whereas the increasing range is so small that it could not qualitatively alter the spike initiation dynamics. These results highlight that neuronal geometric parameter is a crucial factor in determining the spike initiation dynamics to electric fields. The finding is useful to interpret the functional significance of neuronal biophysical properties in their encoding dynamics, which could contribute to uncovering how neuron encodes electric field signals.

Citation: Yi G-S, Wang J, Wei X-L, Tsang K-M, Chan W-L, et al. (2014) Neuronal Spike Initiation Modulated by Extracellular Electric Fields. PLoS ONE 9(5): e97481. doi:10.1371/journal.pone.0097481

Editor: Steven Barnes, Dalhousie University, Canada

Received January 10, 2014; **Accepted** April 20, 2014; **Published** May 29, 2014

Funding: This work is supported by the National Natural Science Foundation of China under Grants 61072012 (URL: http://www.nsfc.gov.cn/publish/portal0/default.htm), 61172009 (URL: http://www.nsfc.gov.cn/publish/portal0/default.htm) and 61372010 (URL: http://www.nsfc.gov.cn/publish/portal0/default.htm), and Tianjin Municipal Natural Science Foundation under Grants 12JCZDJC21100 (URL: http://www.tstc.gov.cn/) and 13JCZDJC27900 (URL: http://www.tstc.gov.cn/). The funders had no role in study design, data collection and analysis, decision to publish, or preparation of the manuscript.

Competing Interests: The authors have declared that no competing interests exist.

* E-mail: xilewei@tju.edu.cn

Introduction

Electromagnetic field stimulation, as a noninvasive brain modulation technique, nowadays has been successfully and widely used in the clinic to treat and study various neurologic, psychiatric and pain disorders [1–3]. The commonly used techniques encompass transcranial magnetic stimulation (TMS), repetitive TMS (rTMS), electroconvulsive therapy (ECT), transcranial direct current stimulation (tDCS), low field magnetic stimulation (LFMS), and so on [1,2,4–7]. This special stimulus modality could induce an electric field in the extracellular space around the interested brain tissue to modulate relevant neuronal activity and ultimate behavior [3,8]. One fundamental question of this technique needed to be solved is that the precise mechanism underlying neuronal excitation by electromagnetic stimulus is still unclear [1–3,8,9]. Addressing this question requires the knowledge of how the induced extracellular electric field interacts with neuronal encoding dynamics [3,8].

There have been many experimental studies regarding the interactions between electric field and neuronal encoding dynamics. It has been shown that extracellular electric field is capable of modulating the excitability of many neurons [10–13]. For example, it could suppress [14,15] and entrain epileptiform activities [16], promote burst firing [9], affect cortical wave propagation [17], and alter action potential threshold or timing [9,18]. Moreover, unlike invasive current stimulus, the electric field stimulus could induce spatial polarization in neurons [9–11,19,20]. The neuronal segments near the stimulating anode are hyperpolarized, and simultaneously the segments near cathode are depolarized. These neuromodulatory effects of electric field are governed by both of electric field characteristics and neuronal physiological properties, especially morphological features [9,19–22]. However, the relevant mechanisms underlying these effects are still unclear.

In fact, how neuron encodes stimulus information has been shown to derive from their spike initiation dynamics [23,24]. It mainly refers to how different membrane variables interact at the subthreshold potentials, which could decipher neuron adopts what rules to determine when and why they spike, i.e., how an individual spike is initiated. In computational neuroscience, the dynamical mechanisms of spike initiation are usually studied with nonlinear dynamical system theory, such as phase plane, stability or bifurcation analysis [23–28]. With these methods, the underlying mechanisms of abundant neuronal properties to external current stimulus are uncovered, such as adaptation [29,30], sensitivity [31], Hodgkin's three classes of excitability

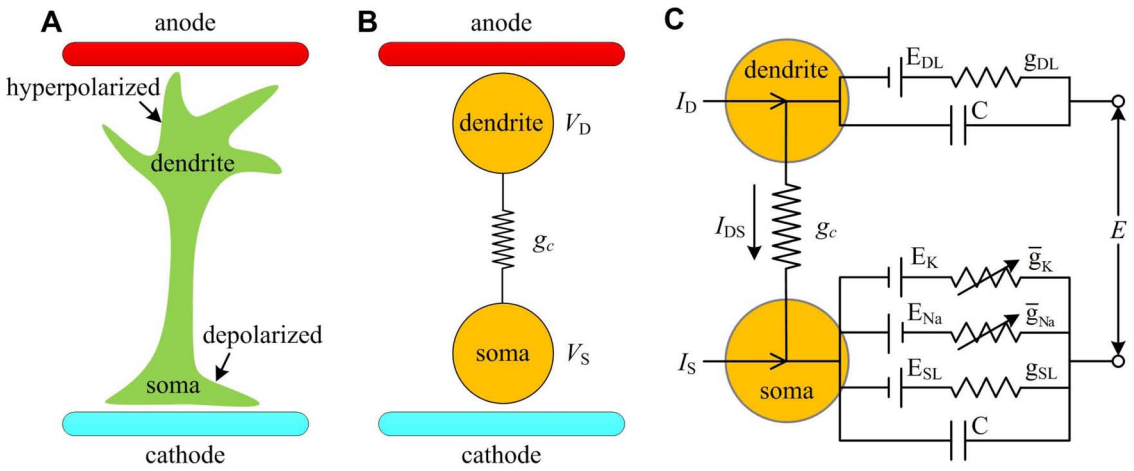

Figure 1. Two-compartment neuron model to extracellular electric fields. (A) A simplified schematic of the spatial polarization in the neuron induced by extracellular electric field. The membrane near the anode is hyperpolarized, which is depolarized near the cathode. (B) To represent this spatial polarization effect, the neuron is replaced by two compartments, which respectively represent soma and dendrite. (C) The currents and conductances for two-compartment neuron. There are Na^+, K^+, passive leakage and capacitive currents in somatic compartment, whereas the dendritic compartment only contains a passive leakage current and a capacitive current.
doi:10.1371/journal.pone.0097481.g001

[24], bursting [26], synchronization [26,27], and so on. Moreover, neuronal encoding schemes to external information are also tightly related to the properties of vast ionic channels in neuron membranes, and many researches adopt it to interpret the biophysical basis of spike initiation. For example, Prescott et al found that the relative activation properties between inward and outward ionic currents could lead to different bifurcation mechanism of spike initiation [24]; Wester and Contreras shown that Na^+ channel inactivation and K^+ channel activation could both control the relationship between spike threshold and the rate of rise of the membrane potential, which plays a crucial role in spike initiation [32]. Thus, translating dynamical explanations of spike initiation into biophysically interpretation could provide greater insight into neural encoding [24]. However, there are still no studies using these methods to investigate the spike initiation dynamics of the neuron to electric fields.

In our previous study [33], we first proposed a reduced two-compartment neuron model to explore how extracellular electric field modulates neuron activity. The model not only can represent the main biophysical characteristics of field effects, i.e., spatial polarization, but also incorporates a geometric parameter which describes the proportion of area occupied by soma. Both of them are crucial factors in determining neuronal response to electric field stimulus [8–11,19–22,34]. What is more, it is very suitable for explaining the dynamical mechanism and relevant biophysical basis for electric field effects. Depending on geometric parameter and internal coupling conductance between two compartments, we have extensively studied the spiking behavior and bifurcation structure of the model to extracellular electric fields. It has been found that varying geometric parameter could switch neuronal bifurcation from Hopf to SNIC, while varying internal coupling conductance could only make spike generation through SNIC bifurcation. Further, we have also shown that the electric field threshold for triggering neuron spiking is determined by geometric parameter, which is consistent with previous experimental [9,21,22] and modeling [8] predictions. However, there is still lack of a complete description of the dynamical mechanisms and especially biophysical basis of neuronal spike initiation to electric fields, which leaves some important questions unanswered. How do two parameters induce different effects on the bifurcation structure of the neuron to electric fields? What biophysical properties are qualitatively affected by geometric parameter to alter the bifurcation structure, and why varying internal coupling conductance could not?

To solve these problems, the study first adopts phase plane and stability analysis to further investigate the dynamical properties of the spike initiation with different geometric and internal coupling parameters. Then, we explore their relevant biophysical basis by analyzing the activation properties of different somatic membrane currents at the subthreshold potentials. All these mechanistic investigations of spike initiation could help us uncover how neuron encodes electric field stimulus.

Model

Previous modeling [34–36] and experimental [9–11,19,20] studies have demonstrated that extracellular electric field could induce spatial polarization in the neuron. The membrane potential near anode is hyperpolarized and near cathode is depolarized, which is shown in Figure 1A. The minimal neuronal unit to represent this spatial polarization should at least have two spatially separated compartments [33,35,36]. In our previous study [33], we proposed a two-compartment model (Figure 1B and 1C) to describe the interactions between extracellular electric field and neuronal activities. It is a reduced version of the Pinsky-Rinzel model [37], which is commonly used to describe the membrane dynamics of pyramidal neuron under electric field stimulus [35,36,38]. Figure 1C shows the currents and conductances for each compartment of the neuron.

The two compartments are soma and dendrite, which are connected by an internal coupling conductance g_c. Their transmembrane potentials are respectively denoted by V_S and V_D, and the equations to describe their states are

$$\begin{aligned} C\frac{dV_S}{dt} = \frac{I_S}{p} + \frac{I_{DS}}{p} - g_{Na}m_\infty(V_S)(V_S - E_{Na}) \\ - g_K w(V_S - E_K) - g_{SL}(V_S - E_{SL}) \end{aligned} \quad (1)$$

$$C\frac{dV_D}{dt}=\frac{I_D}{1-p}-\frac{I_{DS}}{1-p}-g_{DL}(V_D-E_{DL}) \quad (2)$$

The five terms on the right side of equation (1) describe the currents on somatic membrane, which are synaptic input current I_S, internal current I_{DS} that flows from dendrite to soma, inward Na^+, outward K^+ and passive leakage currents, respectively. The three terms on the right side of equation (2) describe the currents on dendritic membrane, which are synaptic input current I_D, internal current I_{DS} and passive leakage current. E_{Na} and E_K are the reversal potentials of Na^+ and K^+ channels on somatic membrane; E_{SL} and E_{DL} are the reversal potentials of leakage channel on somatic and dendritic membrane; $\bar{g}_{Na}$, $\bar{g}_K$, g_{SL} and g_{DL} are the corresponding maximum conductances; C is the membrane capacitance; p and $1-p$ are geometric parameters that respectively characterize the proportion of area occupied by the soma and dendrite.

In equation (1), w is the activation variable for K^+ current, which represents the probability of activation gate being in the open state for K^+ channel. It is governed by

$$\frac{dw}{dt}=\varphi\frac{w_\infty(V_S)-w}{\tau_w(V_S)} \quad (3)$$

where $w_\infty(V_S)$ and $\tau_w(V_S)$ are the steady-state value and time constant for variable w. Moreover, $m_\infty(V_S)$ in equation (1) is the steady-state value of the probability of Na^+ channel being in the open state. $m_\infty(V_S)$, $w_\infty(V_S)$ and $\tau_w(V_S)$ are all functions of somatic membrane potential V_S, which can be described by

$$\begin{cases} m_\infty(V_S)=0.5\left[1+\tanh\left(\frac{V_S+1.2}{18}\right)\right] \\ w_\infty(V_S)=0.5\left[1+\tanh\left(\frac{V_S}{10}\right)\right] \\ \tau_w(V_S)=1\Big/\cosh\left(\frac{V_S}{20}\right) \end{cases} \quad (4)$$

The orientation of extracellular electric field E in our model is parallel to the somatic-dendritic axis, which is in accordance with most experimental studies of individual pyramidal cells to electric fields [18,20,39–42]. The electric field E could induce a polarization between two neuronal compartments and modulate internal current I_{DS} [33,35,36]. Without electric field E, the internal current is $I_{DS}=g_c(V_D-V_S)$. For the neuron in the presence of extracellular electric field, the internal current I_{DS} can be expressed as

$$I_{DS}=g_c(V_D+E-V_S) \quad (5)$$

Since we focus on the spike initiation dynamics of the neuron to extracellular electric fields, the synaptic current I_S and I_D are respectively set to $0\ \mu A/cm^2$ in the following study. The numerical values of the parameters in equations (1)–(5) are shown in Table 1 [33].

Through our previous study, it is found that neuron can generate subcritical Hopf bifurcation (HB1), supercritical Hopf bifurcation (HB2) and saddle-node on invariant circle (SNIC) bifurcation as geometric parameter p changes, while it can only generate SNIC bifurcation as internal coupling conductance g_c changes [33]. The corresponding two-parameter bifurcation diagrams are shown in Figures 2A and 2B. The bifurcation curve divides the (p, E) and (g_c, E) parameter space into two regions, i.e., region I and II. In region I, neuron is in quiescent state, and in region II it exhibits repetitive spiking behavior (Figure 2C). Moreover, there are two different quiescent states, which are depolarized quiescence and hyperpolarized quiescence (Figure 2C). Since there is only a leakage current in dendritic compartment, it cannot generate spike in the observed range of E, which at most exhibits subthreshold oscillation along with V_S (Figure 2C).

Results

Dynamical properties of neuronal spike initiation to extracellular electric field with different geometric parameters

As geometric parameter p changes from 0 to 1, the neuron can generate three types of bifurcation to extracellular electric fields. The corresponding sample one-parameter bifurcation diagrams are shown in Figure 3. For $0.06\le p<0.12$, neuron first generates repetitive spiking through a subcritical Hopf bifurcation (HB1), and then cease this repetitive behavior through a supercritical Hopf bifurcation (HB2) when electric field E changes from 0 mV to 150 mV (Figure 3A). For $0.12\le p<0.15$, neuron generates repetitive spiking through a subcritical Hopf bifurcation (HB1) and never stops this behavior for $E\le 150$ mV (Figure 3B). However, the neuron generates repetitive spiking through a SNIC bifurcation for $0.15\le p<0.84$ and keeps on spiking when $E\le 150$ mV (Figure 3C). When geometric parameter p is too high or too low, such as $p<0.06$ or $p\ge 0.84$, there is no bifurcation occurring for $0\ \text{mV}\le E\le 150\ \text{mV}$. Next, we will use stability and phase plane analysis to further investigate the dynamical properties of the spike initiation in these three cases.

To facilitate stability analysis, we rewrite our two-compartment neuron in the following form

$$\begin{cases} f_1=\frac{dV_S}{dt} \\ f_2=\frac{dV_D}{dt} \\ f_3=\frac{dw}{dt} \end{cases} \quad (6)$$

At the equilibrium points of the neuron, there is

$$\begin{cases} f_1=0 \\ f_2=0 \\ f_3=0 \end{cases} \quad (7)$$

The Jacobian matrix of the neuron at the equilibrium point has the following form

$$J=\begin{bmatrix} \frac{\partial f_1}{\partial V_S} & \frac{\partial f_1}{\partial V_D} & \frac{\partial f_1}{\partial w} \\ \frac{\partial f_2}{\partial V_S} & \frac{\partial f_2}{\partial V_D} & \frac{\partial f_2}{\partial w} \\ \frac{\partial f_3}{\partial V_S} & \frac{\partial f_3}{\partial V_D} & \frac{\partial f_3}{\partial w} \end{bmatrix} \quad (8)$$

Table 1. Numerical values for the parameters in the two-compartment model.

Parameters	Values	Parameters	Values
C	$2\ \mu F/cm^2$	$\bar{g}_{Na}$	$20\ mS/cm^2$
E_{Na}	50 mV	$\bar{g}_K$	$20\ mS/cm^2$
E_K	−100 mV	g_{SL}	$2\ mS/cm^2$
E_{SL}	−70 mV	g_{DL}	$2\ mS/cm^2$
E_{DL}	−70 mV	ϑ	0.15 (unitless)

doi:10.1371/journal.pone.0097481.t001

For f_1, f_2 and f_3, we have

$$f_1:\begin{cases}\frac{\partial f_1}{\partial V_S}=\frac{1}{C}\left[-\frac{g_c}{p}-g_{Na}m_\infty(V_S)-g_{Na}m'_\infty(V_S)(V_S-E_{Na})-g_K w-g_{SL}\right]\\ \frac{\partial f_1}{\partial V_D}=\frac{1}{C}\frac{g_c}{p}\\ \frac{\partial f_1}{\partial w}=-\frac{g_K}{C}(V_S-E_K)\end{cases}\tag{9}$$

where $m'_\infty(V_S)=\frac{dm_\infty(V_S)}{dV_S}$.

$$f_2:\begin{cases}\frac{\partial f_2}{\partial V_S}=\frac{1}{C}\frac{g_c}{1-p}\\ \frac{\partial f_2}{\partial V_D}=\frac{1}{C}\left(-\frac{g_c}{1-p}-g_{DL}\right)\\ \frac{\partial f_2}{\partial w}=0\end{cases}\tag{10}$$

$$f_3:\begin{cases}\frac{\partial f_3}{\partial V_S}=\varphi\frac{w'_\infty(V_S)\tau_w(V_S)-[w_\infty(V_S)-w]\tau'_w(V_S)}{\tau_w{}^2(V_S)}\\ \frac{\partial f_3}{\partial V_D}=0\\ \frac{\partial f_3}{\partial w}=-\frac{\vartheta}{\tau_w(V_S)}\end{cases}\tag{11}$$

where $w'_\infty(V_S)=\frac{dw_\infty(V_S)}{dV_S}$ and $\tau'_w(V_S)=\frac{d\tau_w(V_S)}{dV_S}$.

From $f_3=0$ in equation (7), we have $w=w_\infty(V_S)$ at the equilibrium point. Taking this condition into $\frac{\partial f_1}{\partial V_S}$ and $\frac{\partial f_3}{\partial V_S}$, we could obtain the following two equations,

$$\begin{cases}\frac{\partial f_1}{\partial V_S}=\frac{1}{C}\left[-\frac{g_c}{p}-g_{Na}m_\infty(V_S)-g_{Na}m'_\infty(V_S)(V_S-E_{Na})-g_K w_\infty(V_S)-g_{SL}\right]=Q\\ \frac{\partial f_3}{\partial V_S}=\phi\frac{w'_\infty(V_S)}{\tau_w(V_S)}\end{cases}\tag{12}$$

Substituting equations (9)–(12) into the Jacobian matrix (8), we could obtain

$$J=\begin{bmatrix}Q & \frac{1}{C}\frac{g_c}{p} & -\frac{\bar{g}_K}{C}(V_S-E_K)\\ \frac{1}{C}\frac{g_c}{1-p} & \frac{1}{C}\left(-\frac{g_c}{1-p}-g_{DL}\right) & 0\\ \varphi\frac{w'_\infty(V_S)}{\tau_w(V_S)} & 0 & -\frac{\varphi}{\tau_w(V_S)}\end{bmatrix}\tag{13}$$

When $p=0.09$, neuron generates the left bifurcation (HB1) at $E=45.7174$ mV. By solving nonlinear equations (7) at this electric

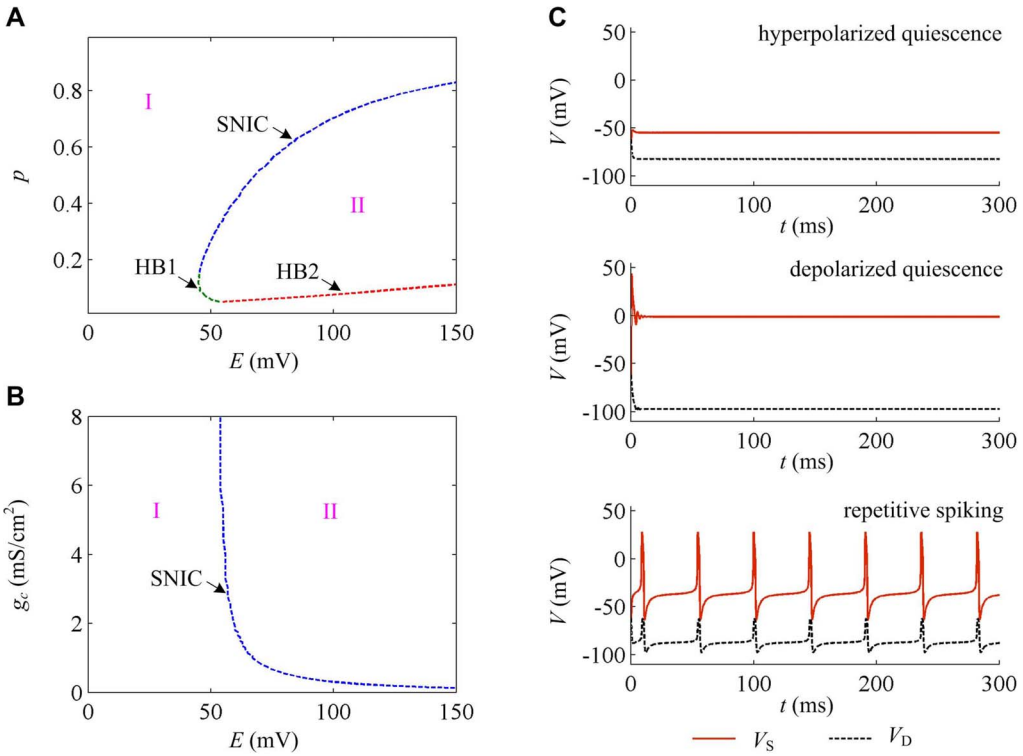

Figure 2. Dynamical properties of the neuron to electric fields. (A) Two-parameter bifurcation diagram in (p, E) parameter space. (B) Two-parameter bifurcation diagram in (g_c, E) parameter space. (C) Different spiking behaviors exhibited by the neuron to electric fields. In (A) and (B), region I indicates quiescent state and region II indicates repetitive spiking state. 'HB1' refers to subcritical Hopf bifurcation, 'HB2' refers to supercritical Hopf bifurcation, and 'SNIC' refers to saddle-node on invariant circle bifurcation.
doi:10.1371/journal.pone.0097481.g002

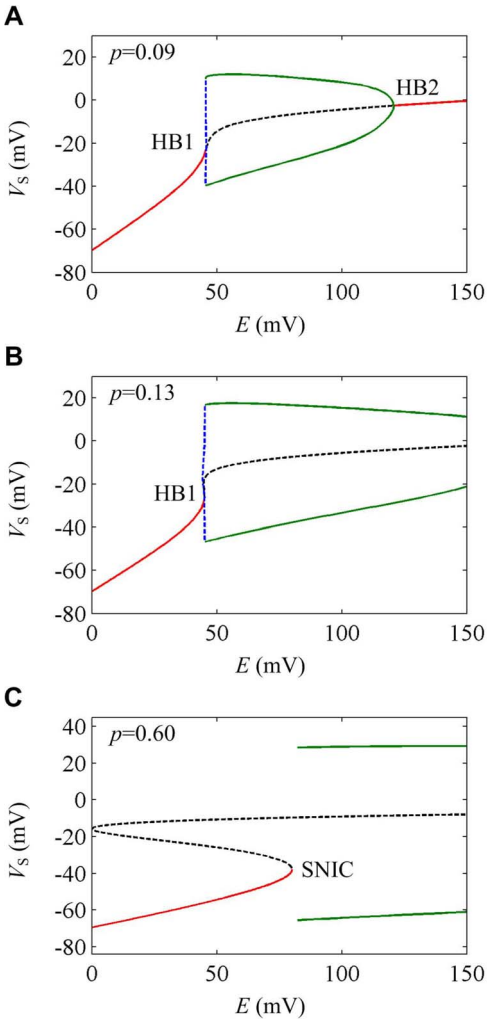

Figure 3. Three types of one-parameter bifurcation by varying geometric parameter. The bifurcation parameter is electric field E and the geometric parameter is (A) $p=0.09$, (B) $p=0.13$ and (C) $p=0.60$, respectively. The stable equilibrium is indicated by red solid line and unstable one is black dotted line. The stable limit cycle is indicated by green solid line and unstable one is blue dotted line.
doi:10.1371/journal.pone.0097481.g003

field intensity, it is found the equilibrium of the neuron is $(V_{S0},V_{D0},w_0)=(-22.7563\ \text{mV},-69.4588\ \text{mV},0.0104)$. Then, the characteristic polynomial of Jacobian matrix $\mathcal{J}$ is $\lambda^3+3.1134\lambda^2+0.1197\lambda+0.3728=0$. The corresponding characteristic eigenvalues are $\lambda_{1,2}=\pm 0.3460\text{i}$ and $\lambda_3=-3.1134$. There is a pair of purely imaginary eigenvalues, which corresponds to the non-hyperbolicity condition of Hopf bifurcation [23]. Since there is unstable limit cycle appearing (Figure 3A), the relevant Hopf bifurcation is subcritical. With $E=120.7150\ \text{mV}$, the neuron generates the right bifurcation (HB2). At this electric field intensity, the equilibrium of the neuron is $(V_{S0},V_{D0},w_0)=(-2.5277\ \text{mV},-88.8804\ \text{mV},0.3762)$, and the characteristic polynomial of Jacobian matrix $\mathcal{J}$ is $\lambda^3+2.1385\lambda^2+4.8439\lambda+10.3592=0$. Its corresponding characteristic eigenvalues are $\lambda_{1,2}=\pm 2.2009\text{i}$ and $\lambda_3=-2.1386$. Thus, the right bifurcation is also a Hopf bifurcation [23]. But unlike HB1, there is a stable limit cycle appearing (Figure 3A), so the relevant Hopf bifurcation is supercritical.

Figure 4A shows the phase plane analysis of the spike initiation dynamics in the case of $p=0.09$. Since the dendritic compartment only contains a passive leakage current and does not include other ionic currents, the spiking initiation dynamics of the neuron are mainly controlled by the interactions between somatic membrane potential V_S and its K^+ channel activation variable w. Therefore, although there are three dynamical variables in our model, we could perform phase plane analysis on (w, V_S) plane (Figure 4). When $E<45.7174\ \text{mV}$, the V_S- and w-nullclines interact at a stable fixed point (left panel, Figure 4A). All the V_S-trajectories converge to this stable intersection, so the neuron is at the resting state and there is no repetitive spike generating. The nullcline in phase space for a variable represents the states where the variable neither increases nor decreases [23]. The interaction of two variable nullclines is the equilibrium of the neuron. The increase of electric field E has no effects on w-nullcline, but could shift the V_S-nullcline to the upper right. Once $E>45.7174\ \text{mV}$, the fixed point is destabilized, and meanwhile there is a stable limit cycle appearing (center panel, Figure 4A). All the V_S-trajectories converge to this stable limit cycle and neuron begins to spike repetitively. The destabilization of the fixed point and the appearance of repetitive spiking in this process are accomplished by subcritical Hopf bifurcation. Then, the V_S-nullcline continues to move to the upper right as E further increases. Once $E>120.7150\ \text{mV}$, the interaction between V_S- and w-nullclines changes to a stable fixed point once more, meanwhile the stable limit cycle disappears (right panel, Figure 4A). In this case, the V_S-trajectories converge to this stable fixed point and repetitive spiking ceases. The stabilization of the fixed point and the qualitative change in neuronal behavior are accomplished by supercritical Hopf bifurcation. Moreover, the stable fixed point is in the suprathreshold range, so the neuron exhibits depolarized quiescent state (center panel, Figure 2C).

When $p=0.13$, neuron generates bifurcation (HB1) at $E=45.0620\ \text{mV}$. The corresponding characteristic eigenvalues of Jacobian matrix $\mathcal{J}$ are $\lambda_{1,2}=\pm 0.1827\text{i}$ and $\lambda_3=-2.6973$. Hence, there is a Hopf bifurcation taking place in the neuron [23]. Since the limit cycle appearing in this process is unstable (Figure 3B), the Hopf bifurcation is subcritical. From the phase portraits in Figure 4B, the interaction between V_S- and w-nullclines changes from a stable fixed point to unstable when the bifurcation occurs. Meanwhile, a stable limit cycle appears in the phase portrait which corresponds to repetitive spiking behavior. Unlike the case of $p=0.09$, the unstable fixed point does not stabilize again and the stable limit cycle always exists for $E\le 150\ \text{mV}$. Therefore, the neuron keeps on repetitive spiking in the observed range of E.

For $p=0.60$, neuron generates bifurcation at $E=80.0803\ \text{mV}$. The corresponding characteristic eigenvalues of Jacobian matrix $\mathcal{J}$ are $\lambda_1=-2.6998$, $\lambda_2=5.4648\text{e}-06\approx 0$ and $\lambda_3=-0.4584$. Apparently, this satisfies the non-hyperbolicity condition of the saddle-node bifurcation [23]. From the phase portraits in Figure 4C, it is found there are three interactions between V_S- and w-nullclines when $E<80.0803\ \text{mV}$. Since the leftmost fixed point is stable and the other two are unstable, neuron exists in quiescent state. As electric field E increases, the V_S-nullcline shifts to the upper right and the distance between the left two intersections gets closer. Once $E>80.0803\ \text{mV}$, these two intersections coalesce and annihilate each other. Meanwhile, a stable limit cycle appears and neuron begins to spike repetitively. This process corresponds to the SNIC bifurcation. After that, the V_S- and w-nullclines always interact at an unstable fixed point and the stable limit cycle always exists in the observed range of E. So the neuron always exhibits repetitive spiking for $E\le 150\ \text{mV}$.

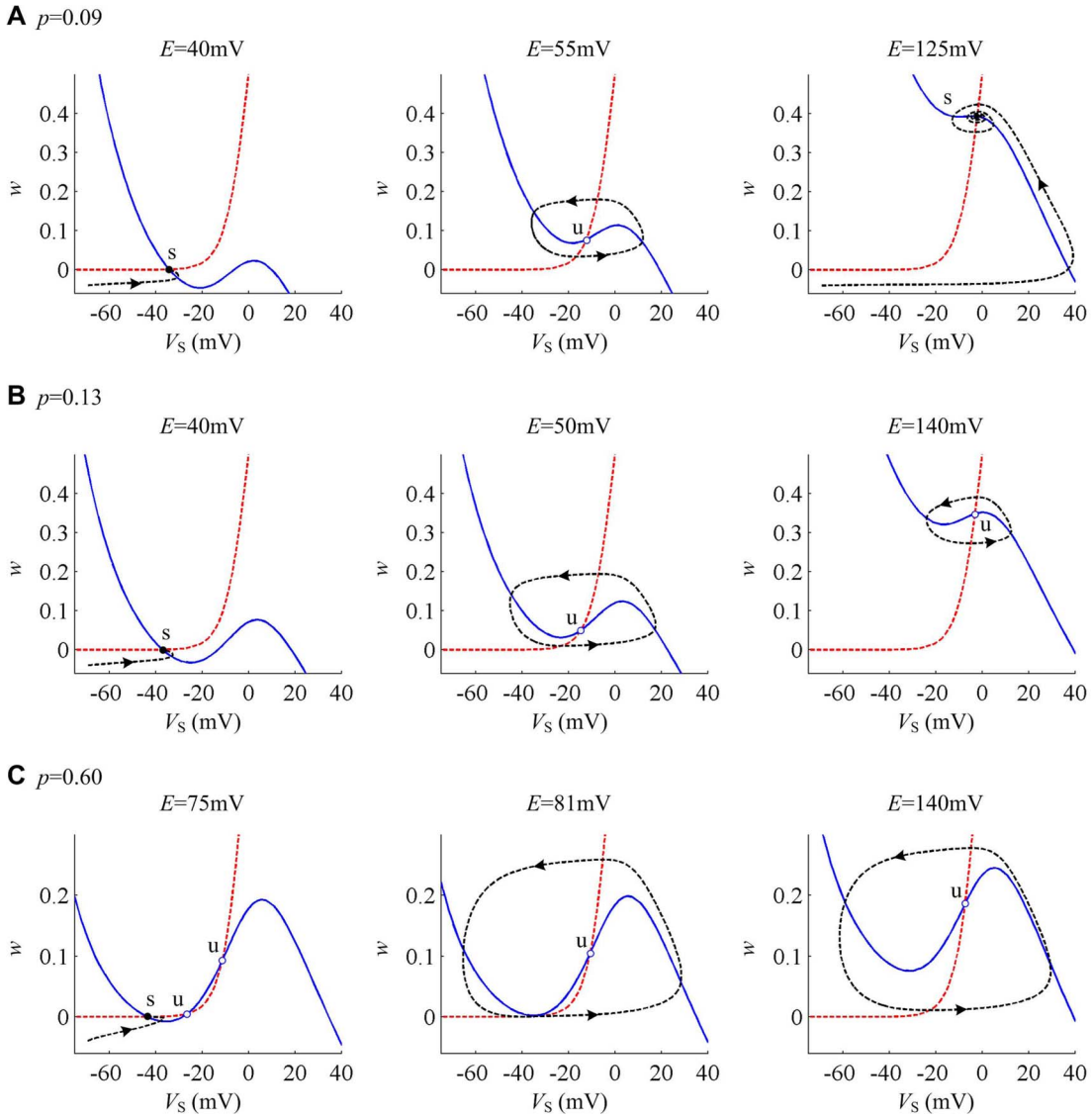

Figure 4. Phase plane analysis about (w, V_S) with different geometric parameters. The geometric parameter is (A) $p=0.09$, (B) $p=0.13$ and (C) $p=0.60$, respectively. The blue solid line represents V_S-nullcline and red dotted line is w-nullcline. The black dotted line is a sample V_S trajectory, where arrow indicates the direction of its motion. 's' indicates stable equilibrium and 'u' is unstable.
doi:10.1371/journal.pone.0097481.g004

Dynamical properties of neuronal spike initiation to extracellular electric field with different internal coupling conductances

As internal coupling conductance g_c changes, the neuron can only generate SNIC bifurcation to extracellular electric fields. The corresponding sample one-parameter bifurcation diagrams are shown in Figure 5. That is, the internal coupling conductance g_c can only change the electric field value at the bifurcation point, which cannot alter the bifurcation type.

For $g_c=0.8\ \mathrm{mS/cm^2}$, neuron generates bifurcation at $E=72.1409\ \mathrm{mV}$. The corresponding characteristic eigenvalues of Jacobian matrix $\mathcal{J}$ are $\lambda_1=-2.1405$, $\lambda_2=3.1062\mathrm{e}-06\approx 0$ and $\lambda_3=-0.4371$. For $g_c=1.5\ \mathrm{mS/cm^2}$, neuron generates bifurcation at $E=62.0812\ \mathrm{mV}$. The corresponding characteristic eigenvalues of Jacobian matrix $\mathcal{J}$ are $\lambda_1=-3.3718$, $\lambda_2=-3.9529\mathrm{e}-06\approx 0$ and $\lambda_3=-0.4022$. Since each case has a zero characteristic eigenvalue, the corresponding bifurcations are both SNIC bifurcation [23].

Whether $g_c=0.8\ \mathrm{mS/cm^2}$ or $g_c=1.5\ \mathrm{mS/cm^2}$, it can be observed that the interactions between V_S- and w-nullclines both have three fixed points before bifurcation occurs from the phase portraits in Figure 6. When the bifurcation takes place, the left two fixed points coalesce and annihilate each other. Then, two nullclines interact at only an unstable point. Since there is a stable limit cycle simultaneously appearing, neuron starts to spike repetitively. This process corresponds to the SNIC bifurcation. For $E\leq 150\ \mathrm{mV}$, the stable limit cycle always exists in the phase portraits and the neuron always exhibits repetitive spiking.

Biophysical basis of the spiking initiation dynamics modulated by extracellular electric fields

The neuronal membrane currents with different directions, i.e., inward or outward, could produce different effects on membrane

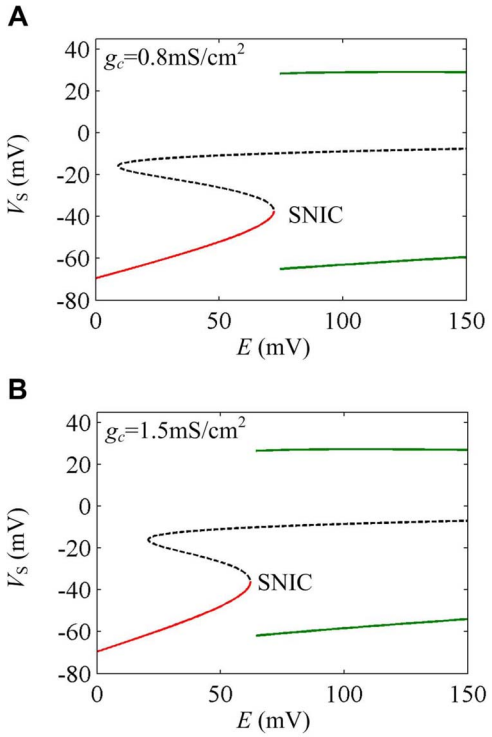

Figure 5. Two sample one-parameter bifurcation diagrams by varying internal coupling conductance. The bifurcation parameter is electric field E and the internal coupling conductance is (A) $g_c = 0.8$ mS/cm^2 and (B) $g_c = 1.5$ mS/cm^2. The stable equilibrium is indicated by red solid line and unstable one is black dotted line. The stable limit cycle is indicated by green solid line and unstable one is blue dotted line.
doi:10.1371/journal.pone.0097481.g005

potentials. The inward current mainly leads to the depolarization of membrane potential, while the outward current mainly hyperpolarizes membrane potential [23,24,43]. The relative activation properties at the subthreshold potentials between inward and outward currents are tightly related to the dynamical bifurcation of the neuron [24]. When SNIC bifurcation takes place, the outward current is very weak or has not yet been activated at perithreshold potentials, and the activated inward current could drive membrane potential to slowly pass through threshold without competition, which enables neuron to maintain slow repetitive spiking. On the contrary, when Hopf bifurcation occurs, the outward current is relatively strong or has been activated at perithreshold potentials. To generate action potential, the inward current must be activated more rapidly and outrun the outward current to produce suprathreshold depolarization. To summary, a relative increase in outward current encourages the occurrence of Hopf bifurcation, and a relative increase in inward current encourages the occurrence of SNIC bifurcation [24,43]. Moreover, it is found that the relation between steady-state membrane current I and membrane potential V (i.e., I-V curve) in the absence of external stimulus could qualitatively reflect the nonlinear competition between inward and outward currents [23,24]. Specifically, a Hopf bifurcation corresponds to a monotonic I-V curve, whereas SNIC bifurcation corresponds to a non-monotonic I-V curve which has a local maximum value. Thus, to explore the biophysical basis of the spike initiation dynamics modulated by electric fields, we could analyze the activation properties of inward and outward membrane currents at the subthreshold potentials as well as the steady-state I-V curve properties in the case of different geometric and internal coupling parameters.

Since the dendrite only contains a leakage current, we focus on the relation between somatic steady-state membrane current I_{SS} and its membrane potential V_S (I_{SS}-V_S curve). The somatic steady-state membrane current I_{SS} is defined as the sum of currents in somatic chamber, which can be written as

$$I_{SS} = I_{Na} + I_K + I_{SL} + I_o \tag{14}$$

where $I_{Na} = \bar{g}_{Na} m_\infty(V_S)(V_S - E_{Na})$ is the steady-state Na^+ current, $I_{SL} = g_{SL}(V_S - E_{SL})$ is the leakage current. Since there is $w = w_\infty(V_S)$ at steady state, the steady-state K^+ current becomes $I_K = \bar{g}_K w_\infty(V_S)(V_S - E_K)$. $I_o = -I_{DS}/p$ is the steady-state internal current that flows from soma to dendrite and the geometric parameter should be included. In the absence of electric field, i.e., $E = 0$ mV, according to $f_2 = 0$ [equation (7)], we have

$$V_D = \frac{(1-p)g_{DL}E_{DL} + g_c V_S}{g_c + (1-p)g_{DL}} \tag{15}$$

Then, the steady-state internal current I_o in equation (14) becomes

$$I_o = -\frac{I_{DS}}{p} = -\frac{g_c(V_D - V_S)}{p} = -\frac{g_c g_{DL}(1-p)(E_{DL} - V_S)}{p[g_c + (1-p)g_{DL}]} \tag{16}$$

For somatic chamber, this is an outward current.

From the expressions of steady-state Na^+ current I_{Na}, K^+ current I_K and leakage current I_{SL}, it can be found that all of them do not contain geometric parameter p and internal coupling conductance g_c. Thus, the change of these two parameters cannot alter the activation properties of I_{Na}, I_K and I_{SL} at the subthreshold potentials (Figure 7A). From the results in Figure 7A, we can also observe that the inward I_{Na} is activated at lower V_S than outward I_K.

However, both of geometric parameter p and internal coupling conductance g_c could affect the activation property of internal current I_o at subthreshold potentials, which are shown in Figures 7B and 7C. When the geometric parameter p is low, the intensity of the internal current I_o flowing out of soma is very large ($p = 0.09$, Figure 7B). In this case, although inward I_{Na} is activated at lower V_S than outward I_K, the high intensity outward I_o makes the total outward current become much stronger than inward current at perithreshold potentials, which encourages the occurrence of Hopf bifurcation. From Figure 7D, it can be found the I_{SS}-V_S curve in this case is monotonic and does not have local maximum value. Thus, the spike initiation is generated through a Hopf bifurcation (Figure 3A). As geometric parameter p increases, the intensity of outward I_o gets smaller, whereas the activation property of inward current I_{Na} remains unchanged, which leads to a relative decrease in outward current. Once p exceeds a critical value, the I_{SS}-V_S curve changes from monotonic to non-monotonic, which has a local maximum value ($p = 0.30$, Figure 7D). It indicates that the outward current in this case cannot out-compete inward current at perithreshold potentials, and then the membrane potential could be forced to slowly pass through threshold by activated inward I_{Na}. Thus, the spike initiation of the neuron to electric field is switched from Hopf bifurcation to SNIC bifurcation. As p further increases, the

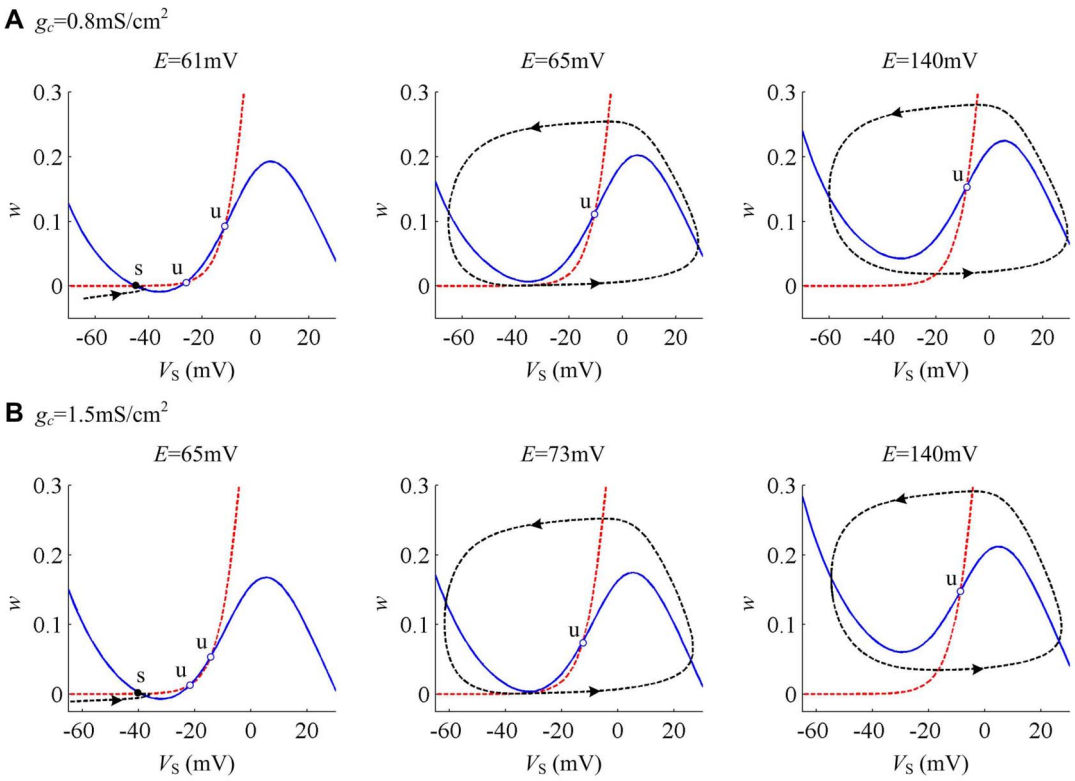

Figure 6. Phase plane analysis about (w, V_S) with different internal coupling conductances. The internal coupling conductance is (A) $g_c = 0.8$ mS/cm^2 and (B) $g_c = 1.5$ mS/cm^2. Blue solid line represents V_S-nullcline and red dotted line is w-nullcline. Black dotted line is a sample V_S trajectory, where arrow indicates its direction of motion. 's' indicates stable equilibrium and 'u' is unstable.
doi:10.1371/journal.pone.0097481.g006

intensity of outward I_o gets even smaller ($p = 0.60$, Figure 7B), which leads to a bigger decrease in outward current relative to inward I_{Na}. In this case, the I_{SS}-V_S curve keeps non-monotonic ($p = 0.60$, Figure 7D), which corresponds to a SNIC bifurcation (Figure 3C).

On the contrary, the intensity of outward current I_o increases as internal coupling conductance g_c increases (Figure 7C). However, compared with the case of geometric parameter p, the increasing range is much smaller, which could not qualitatively alter the nonlinear competition between inward and outward currents. In this case, the I_{SS}-V_S curves for different g_c values are always non-monotonic (Figure 7E). Thus, the neuron could only generate SNIC bifurcation to electric fields as g_c changes (Figure 5).

Conclusions

Based on a reduced two-compartment model, we have studied the dynamical and biophysical mechanism of neuronal spike initiation to extracellular electric fields in this paper. In our previous study [33], it has been shown that this model could generate different bifurcations (i.e., Hopf or SNIC bifurcation) to electric fields as geometric parameter changes, whereas it could only generated SNIC bifurcation as internal coupling conductance changes. However, it still lacks of a complete description of how varying two parameters induce different effects on neuronal spiking initiation dynamics to electric fields.

In this study, we first use stability theory and phase plane analysis to further investigate the dynamical properties of spike initiation induced by these two parameters in detail. It has been shown that geometric parameter variation could lead to different types of characteristic eigenvalues of the Jacobian matrix appearing at the equilibrium point, whereas internal coupling conductance could not. With phase plane analysis, it is shown that varying geometric parameter could alter the mode of interactions between V_S- and w-nullclines on the phase portraits, whereas varying another parameter could not. All these results show that the geometric parameter could qualitatively alter the dynamical properties and bifurcation mechanisms of neuronal spike initiation modulated by extracellular electric fields.

Then, we explore the biophysical basis of spike initiation dynamics of the neuron to electric fields. By analyzing the activation properties of inward and outward membrane currents at the subthreshold potentials, it is found that geometric parameter and internal coupling conductance do not affect the activation properties of somatic Na^+, K^+ and leakage currents, whereas they could alter the intensity of the internal current flowing from soma to dendrite. Specifically, the internal current intensity greatly decreases as geometric parameter increases, which makes the spike initiation mechanism switch from Hopf bifurcation to SNIC bifurcation. Although the internal current intensity increases as internal coupling conductance increases, the increasing range is much smaller relative to the case of geometric parameter, which could not qualitatively alter the nonlinear competition between inward and outward currents. Then, the spike initiation could occur only through SNIC bifurcation. Hence, it can be concluded that geometric parameter could greatly change the internal current intensity to qualitatively alter the dynamical mechanism of neuronal spike initiation, which further highlight the spatial polarization effects of extracellular electric field. All these findings demonstrate that geometric parameter is a crucial factor in

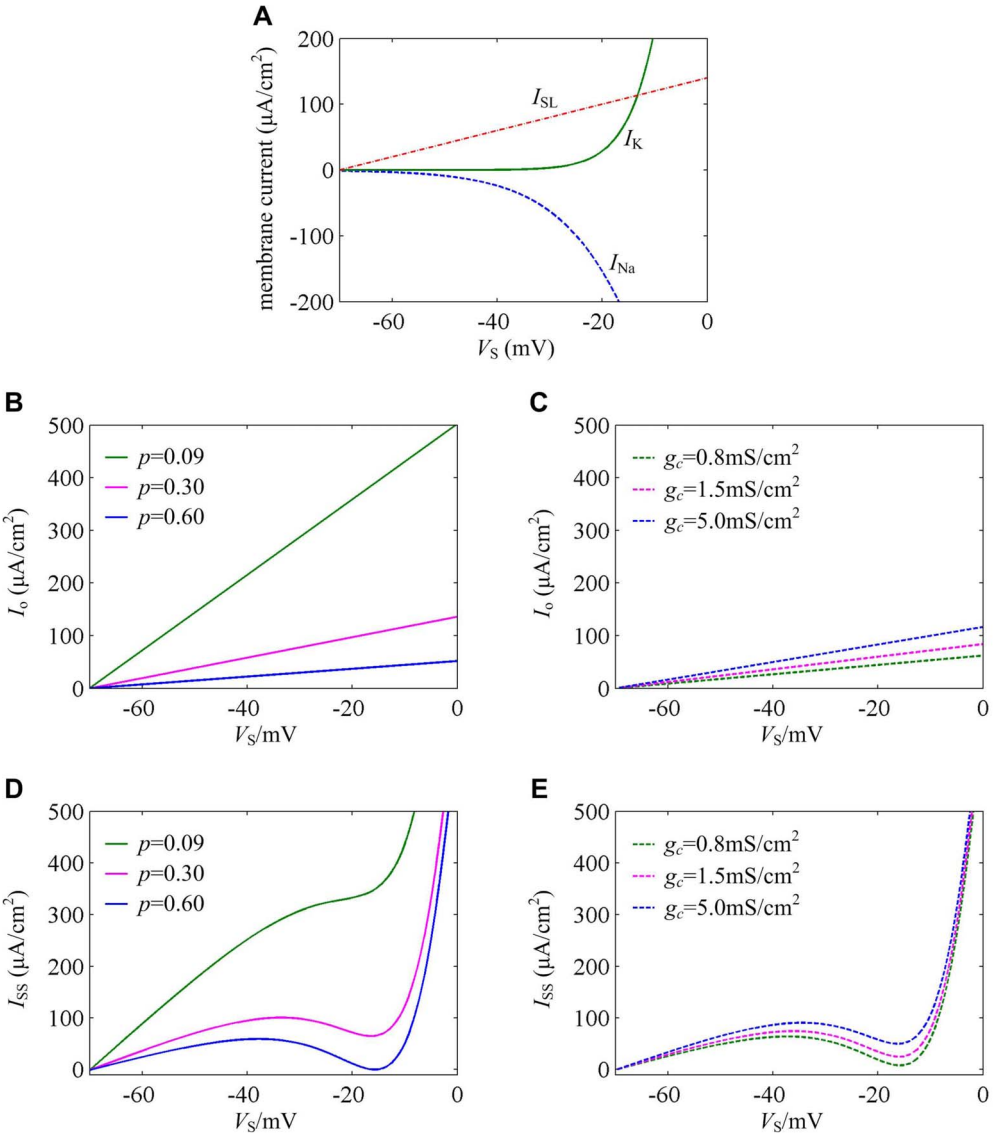

Figure 7. Activation properties of somatic membrane currents at the subthreshold potentials. (A) The relation between somatic I_{Na}, I_K, I_{SL} currents and its membrane potential V_S at the subthreshold potentials. The activations of these three currents are all not affected by geometric parameter and internal coupling conductance. (B) The relation between the internal current I_o flowing from soma to dendrite and somatic membrane potential V_S (I_o-V_S curve) at the subthreshold potentials with $p = 0.09$, 0.30 and 0.60. (C) I_o-V_S curves at the subthreshold potentials with $g_c = 0.8$ mS/cm^2, 1.5 mS/cm^2 and 5.0 mS/cm^2. (D) I_{SS}-V_S curves at the subthreshold potentials with $p = 0.09$, 0.30 and 0.60. (E) I_{SS}-V_S curves at the subthreshold potentials with $g_c = 0.8$ mS/cm^2, 1.5 mS/cm^2 and 5.0 mS/cm^2.
doi:10.1371/journal.pone.0097481.g007

determining neuronal spike initiation dynamics to electric fields. In previous experimental and modeling studies, it has been proposed that morphological feature plays a key role in neuromodulatory effects of electric field. For instance, it could not only determine the electric field threshold for triggering action potentials [8,9,18,20–22], but also control the spatial polarization effects induced by electric field [9,19,20,34]. Thus, our results could provide further support for these previous proposals from the spike initiation dynamical point of view.

In addition, our work describes a connection between neuronal biophysical properties and their spike initiation dynamics to electric fields, which is useful to interpret the functional significance of these properties in neural coding. To our knowledge, this is the first study to explore the biophysical basis of spike initiation of the neuron to electric field stimulus. The results could be used to give some general explanations of the corresponding experimental phenomena under electric field stimulus, which in turn could be tested by experimental recording. Moreover, our reduced two-compartment model and modeling approach as well as analysis method could also provide a new perspective to uncover the underlying mechanism of how neuron encodes external electric field stimulus.

Author Contributions

Conceived and designed the experiments: G-SY JW X-LW K-MT W-LC BD. Performed the experiments: G-SY JW X-LW BD. Analyzed the data: G-SY JW X-LW. Contributed reagents/materials/analysis tools: G-SY JW X-LW K-MT W-LC BD. Wrote the paper: GS-Y JW X-LW.

References

1. Wagner T, Valero-Cabre A, Pascual-Leone A (2007) Noninvasive human brain stimulation. Annu Rev Biomed Eng 9: 527–565.
2. Walsh V, Cowey A (2000) Transcranial magnetic stimulation and cognitive neuroscience. Nat Rev Neurosci 1(1): 73–79.
3. Peterchev AV, Wagner TA, Miranda PC, Nitsche MA, Paulus W, et al. (2012) Fundamentals of transcranial electric and magnetic stimulation dose: Definition, selection, and reporting practices. Brain Stimul 5(4): 435–453.
4. Thomas AW, Graham K, Prato FS, McKay J, Forster PM, et al. (2007) A randomized, double-blind, placebo-controlled clinical trial using a low-frequency magnetic field in the treatment of musculoskeletal chronic pain. Pain Res Manag 12(4): 249–258.
5. Peterchev AV, Rosa MA, Deng ZD, Prudic J, Lisanby SH (2010) ECT stimulus parameters: rethinking dosage. J ECT 26(3): 159–174.
6. Nitsche MA, Cohen LG, Wassermann EM, Priori A, Lang N, et al. (2008) Transcranial direct current stimulation: State of the art 2008. Brain Stimul 1(3): 206–23.
7. Lazutkin D, Husar P (2010) Modeling of electromagnetic stimulation of the human brain. Conf Proc IEEE Eng Med Biol Soc 2010: 581–584.
8. Pashut T, Wolfus S, Friedman A, Lavidor M, Bar-Gad I, et al. (2011) Mechanisms of magnetic stimulation of central nervous system neurons. PLoS Comput Biol 7(3): e1002022.
9. Radman T, Ramos RL, Brumberg JC, Bikson M (2009) Role of cortical cell type and morphology in sub- and suprathreshold uniform electric field stimulation. Brain Stimul 2(4): 215–228.
10. Chan CY, Houndsgaard J, Nicholson C (1988) Effects of electric fields on transmembrane potential and excitability of turtle cerebellar Purkinje cells in vitro. Journal of Physiology 402: 751–771.
11. Chan CY, Nicholson C (1986) Modulation by applied electric fields of Purkinje and stellate cell activity in the isolated turtle cerebellum. Journal of Physiology 371: 89–114.
12. Bawin SM, Sheppard AR, Mahoney MD, Adey WR (1984) Influences of sinusoidal electric fields on excitability in the rat hippocampal slice. Brain Research Reviews 323(2): 227–237.
13. Jefferys JGR (1981) Influence of electric fields on the excitability of granule cells in guinea-pig hippocampal slices. Journal of Physiology 319: 143–152.
14. Gluckman BJ, Neel EJ, Netoff TI, Ditto WL, Spano ML, et al. (1996) Electric field suppression of epileptiform activity in hippocampal slices. Journal of Neurophysiology 76(6): 4202–4205.
15. Gluckman BJ, Nguyen H, Weinstein SL, Schiff SJ (2001) Adaptive electric field control of epileptic seizures. The Journal of Neuroscience 21(2): 590–600.
16. Sunderam S, Chernyy N, Peixoto N, Mason JP, Weinstein SL, et al. (2009) Seizure entrainment with polarizing low-frequency electric fields in a chronic animal epilepsy model. Journal of Neural Engineering 6(4): 046009.
17. Richardson KA, Schiff SJ, Gluckman BJ (2005) Control of traveling waves in the Mammalian cortex. Physical Review Letters 94(2): 028103.
18. Bikson M, Inoue M, Akiyama H, Deans JK, Fox JE, et al. (2004) Effects of uniform extracellular DC electric fields on excitability in rat hippocampal slices in vitro. J Physiol 557(Pt 1): 175–90.
19. Svirskis G, Baginskas A, Hounsgaard J, Gutman A (1997) Electrotonic measurements by electric field-induced polarization in neurons: theory and experimental estimation. Biophysical Journal 73(6): 3004–3015.
20. Durand DM (2003) Electric field effects in hyperexcitable neural tissue: a review. Radiat Prot Dosimetry 106(4): 325–331.
21. Rotem A, Moses E (2006) Magnetic stimulation of curved nerves. IEEE Transactions on Biomedical Engineering 53(3): 414–420.
22. Rotem A, Moses E (2008) Magnetic stimulation of one-dimensional neuronal cultures. Biophysical Journal 94(12): 5065–5078.
23. Izhikevich EM (2005) Dynamical systems in neuroscience: The geometry of excitability and bursting. London: The MIT Press.
24. Prescott SA, De Koninck Y, Sejnowski TJ (2008) Biophysical basis for three distinct dynamical mechanisms of action potential initiation. PLoS Comput Biol 4(10): e1000198.
25. Nguyen LH, Hong KS, Park S (2012) Bifurcation control of the Morris-Lecar neuron model via a dynamic state-feedback control. Biological Cybernetics 106(10): 587–594.
26. Wang H, Wang Q, Lu Q (2011) Bursting oscillations, bifurcation and synchronization in neuronal systems. Chaos, Solitons & Fractals 44: 667–675.
27. Wang H, Wang Q, Lu Q, Zheng Y (2013) Equilibrium analysis and phase synchronization of two coupled HR neurons with gap junction. Cognitive Neurodynamics 7(2): 121–131.
28. Colwell LJ, Brenner MP (2009) Action potential initiation in the Hodgkin-Huxley model. PLoS Comput Biol 5(1): e1000265.
29. Prescott SA, Ratté S, De Koninck Y, Sejnowski TJ (2006) Nonlinear interaction between shunting and adaptation controls a switch between integration and coincidence detection in pyramidal neurons. J Neurosci 26(36): 9084–9097.
30. Prescott SA, Sejnowski TJ (2008) Spike-rate coding and spike-time coding are affected oppositely by different adaptation mechanisms. J Neurosci 28(50): 13649–13661.
31. Lundstrom BN, Famulare M, Sorensen LB, Spain WJ, Fairhall AL (2009) Sensitivity of firing rate to input fluctuations depends on time scale separation between fast and slow variables in single neurons. Journal of Computational Neuroscience 27(2): 277–290.
32. Wester JC, Contreras D (2013) Biophysical mechanism of spike threshold dependence on the rate of rise of the membrane potential by sodium channel inactivation or subthreshold axonal potassium current. Journal of Computational Neuroscience 35(1): 1–17.
33. Yi GS, Wang J, Wei XL, Tsang KM, Chan WL, et al. (2013) Exploring how extracellular electric field modulates neuron activity through dynamical analysis of a two-compartment neuron model. Journal of Computational Neuroscience. DOI: 10.1007/s10827-013-0479-z
34. Tranchina D, Nicholson C (1986) A model for the polarization of neurons by extrinsically applied electric fields. Biophysical Journal 50(6): 1139–1156.
35. Park EH, So P, Barreto E, Gluckman BJ, Schiff SJ (2003) Electric field modulation of synchronization in neuronal networks. Neurocomputing 52–54: 169–175.
36. Park EH, Barreto E, Gluckman BJ, Schiff SJ, So P (2005) A model of the effects of applied electric fields on neuronal synchronization. Journal of Computational Neuroscience 19(1): 53–70.
37. Pinsky PF, Rinzel J (1994) Intrinsic and network rhythmogenesis in a reduced Traub model for CA3 neurons. Journal of Computational Neuroscience 1(1–2): 39–60.
38. Wei XL, Chen YH, Lu ML, Deng B, Yu HT, et al. (2013) An ephaptic transmission model of CA3 pyramidal cells: an investigation into electric field effects. Cognitive Neurodynamics. DOI: 10.1007/s11571-013-9269-6
39. Ghai RS, Bikson M, Durand DM (2000) Effects of applied electric fields on low-calcium epileptiform activity in the CA1 region of rat hippocampal slices. J Neurophysiol 84(1): 274–280.
40. Deans JK, Powell AD, Jefferys JG (2007) Sensitivity of coherent oscillations in rat hippocampus to AC electric fields. J Physiol 583(Pt 2): 555–565.
41. Reato D, Rahman A, Bikson M, Parra LC (2010) Low-intensity electrical stimulation affects network dynamics by modulating population rate and spike timing. J Neurosci 30(45): 15067–15079.
42. Berzhanskaya J, Chernyy N, Gluckman BJ, Schiff SJ, Ascoli GA (2013) Modulation of hippocampal rhythms by subthreshold electric fields and network topology. Journal of Computational Neuroscience 34(3): 369–389.
43. Prescott SA, Ratté S, De Koninck Y, Sejnowski TJ (2008) Pyramidal neurons switch from integrators in vitro to resonators under in vivo -like conditions. J Neurophysiol 100(6): 3030–3042.